Ayres, G. H. W. Wong, D. V. Goeddel, *ibid.* **74**, 845 (1993).
30. M. Grilli, J. J.-S. Chiu, M. J. Lenardo, *Int. Rev. Cytol.* **143**, 1 (1991); I. Berberich, G. L. Shu, E. A. Clark, *J. Immunol.* **153**, 4357 (1994).
31. J. Gordon, M. J. Millsum, G. R. Guy, J. A. Ledbetter, *J. Immunol.* **140**, 1425 (1988); M. F. Gruber, J. M. Bjorndahl, S. Nakamuar, S. M. Fu, *ibid.* **142**, 4144 (1989); M. K. Spriggs *et al.*, *J. Exp. Med.* **176**, 1543 (1992); P. Lane *et al.*, *ibid.* **177**, 1209 (1993); D. H. Crawford and D. Catovsky, *Immunology* **80**, 40 (1993); A. W. Heath *et al.*, *Cell Immunol.* **152**, 468 (1993); Y.-J. Liu *et al.*, *Nature* **342**, 929 (1989).
32. H. M. Hu, K. O'Rourke, M. S. Boguski, V. M. Dixit, *J. Biol. Chem.* **269**, 30069 (1994).
33. G. Mosialos *et al.*, *Cell* **80**, 389 (1995).
34. J. H. Miller, in *Experiments in Molecular Genetics*, C. S. H. L. Press, Ed. (Cold Spring Harbor Laboratory, Cold Spring Harbor, NY, 1972).
35. We thank P. Svec and T. Hawkins for their help in sequencing and J. Jacob for critical reading of the manuscript. G.C. and Z.-Y. are recipients of an Irvington House Institute fellowship and a Leukemia Society special fellowship, respectively. S.L. is an Arthritis Investigator of the Arthritis Foundation. D.B. is an American Cancer Society Research Professor. A.M.C. is supported by the Medical Scientist Training Program grant 5-T32-GM07367. S.L., A.M.C., and D.I.H. are also supported in part by Biogen, Cambridge, MA. This work was supported by National Institute of Allergy and Infectious Diseases grant A122346 (D.B.) and by National Cancer Institute (NCI) grant R01-CA55713 to S.L.

22 November 1994; accepted 2 February 1995

Crystal Structure of the Tetramerization Domain of the p53 Tumor Suppressor at 1.7 Angstroms

Philip D. Jeffrey, Svetlana Gorina, Nikola P. Pavletich

The p53 protein is a tetrameric transcription factor that plays a central role in the prevention of neoplastic transformation. Oligomerization appears to be essential for the tumor suppressing activity of p53 because oligomerization-deficient p53 mutants cannot suppress the growth of carcinoma cell lines. The crystal structure of the tetramerization domain of p53 (residues 325 to 356) was determined at 1.7 angstrom resolution and refined to a crystallographic *R* factor of 19.2 percent. The monomer, which consists of a β strand and an α helix, associates with a second monomer across an antiparallel β sheet and an antiparallel helix-helix interface to form a dimer. Two of these dimers associate across a second and distinct parallel helix-helix interface to form the tetramer.

The p53 tumor suppressor (*1*), a tetrameric protein that can bind to specific DNA sequences (*2*) and activate gene expression (*3*, *4*), plays a central role in a cell's response to tumorigenic events. p53 can induce cell cycle arrest in response to DNA damage and thus can prevent genetic alterations such as chromosomal rearrangements and gene amplifications (*5*). In addition to coordinating the DNA damage response, p53 can also induce apoptosis in response to the activation of oncogenes such as c-Myc and E1A (*6*). These findings suggest that p53 exerts its tumor suppressing effects by responding to events that may lead to the abnormal proliferation of cells.

The p53 protein has multiple domains with the DNA binding, transactivation, and tetramerization functions residing in separate domains. The sequence-specific DNA binding activity resides in the central portion which folds into a compact structural domain [core domain, residues 102 to 292 (*7*–*9*)]; the transactivation function resides in the loosely folded NH_2-terminal portion [residues 1 to 44 (*3*, *7*)]; and the tetramerization function resides in a structural domain in the COOH-terminal portion of the protein [residues 320 to 356 (*7*, *9*–*11*)]. Consistent with its tetrameric oligomerization state, the p53 protein binds DNA sites that contain four repeats of the pentamer sequence motif Pu-Pu-Pu-C-(A/T) (*2*).

DNA binding and transactivation are the critical mediators of p53's biological effects because tumor-derived p53 mutants defective in suppressing growth are also defective in DNA binding and transactivation (*3*). In vitro, tetramerization is not essential for DNA binding, and the isolated core domain can bind DNA with approximately one-fifth the affinity of intact p53 (*7*). In vivo, however, oligomerization-deficient p53 cannot efficiently transactivate from genomic p53 binding sites in transient transfection assays (*12*), and it cannot suppress the growth of carcinoma cell lines (*12*, *13*). This suggests that there is a tight threshold for in vivo p53 activity and that oligomerization is required to maintain this activity above threshold (*12*). These findings are analogous to those obtained with several tumorigenic mutants of p53 which bind to DNA with reduced affinity but fail to suppress growth in vivo (*14*).

Using a peptide that corresponds to residues 320 to 356 of p53 (*15*), we have obtained three crystal forms of the tetramer and have determined the structure by the multiple isomorphous replacement method (MIR) (*15*). The quaternary structures in the three crystal forms are essentially identical; therefore, our discussion of the tetramer structure will focus on the tetragonal crystal form that diffracts to beyond 1.7 Å resolution and has been refined to a crystallographic *R* factor of 19.2% (Table 1 and Fig. 1).

The crystal structure of the tetramer reveals that the oligomerization domain contains a β strand from residue 326 to 333 and an α helix from residue 335 to 354. The β strand and the α helix form a V-shaped structure with the helix axis being roughly antiparallel to the direction of the β strand. The transition from the β strand to the α helix occurs over a single residue, Gly^{334}, with the backbone amide nitrogen of the glycine making the last β sheet hydrogen bond and the backbone carbonyl making the first α helical hydrogen bond. The backbone conformation ($\phi = 98°$, $\psi = 130°$) in this hinge region is unique to the glycine amino acid, and it is energetically unfavorable for other amino acids. Consistent with its role as a critical hinge residue between the β strand and the α helix, Gly^{334} is conserved across species (*16*) and is one of the few oligomerization domain residues that has been found to be mutated in tumors (*17*). Flanking the Gly^{334} hinge region, there are hydrophobic interactions between the α helix and the β strand involving the side chains of Ile^{332}, Phe^{338}, and Phe^{341}.

The tetramer has 222-point symmetry (three mutually perpendicular twofold rotation axes), with each of the four monomers being in an identical environment (Fig. 2). The tetragonal crystal form has one monomer in the asymmetric unit, and the three twofold symmetry axes of the tetramer coincide with crystallographic symmetry. The twofold axes intersect at the center of the tetramer near the side chain of Leu^{344}. In the

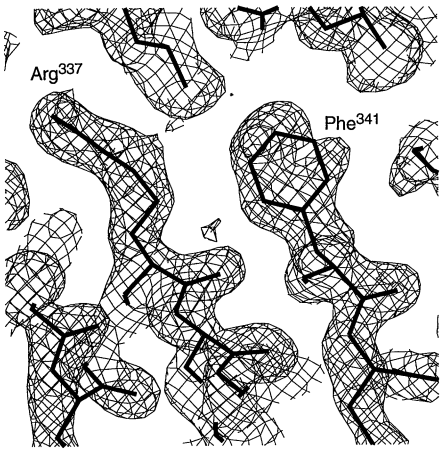

Fig. 1. Multiple isomorphous replacement (MIR) electron density map calculated with phases from the program SQUASH (*34*) at 2.0 Å and contoured at 1.0σ. The Arg^{337} and Phe^{341} residues are labeled. The helix axis is approximately horizontal in the figure.

Cellular Biochemistry and Biophysics Program, Memorial Sloan-Kettering Cancer Center, New York, NY 10021, USA.

Table 1. Data collection and analysis. The peptide of the p53 tetramerization domain crystallizes in space group *P*422 with cell dimensions of $a = b = 45.45$ Å and $c = 33.03$ Å (*15*) and has one monomer in the asymmetric unit. All native and derivative data were collected from the same crystal at room temperature on an RAXIS IIc area detector. Heavy atom derivatives were prepared by successive soaking of the crystal in heavy atom solutions containing 3 M sodium formate, 0.5 M ammonium sulfate, and 100 mM Hepes-Na^+ (pH 7.5) and the following heavy atom compounds: 3 mM silver nitrate for 3 hours (silver-1 derivative); 6 mM silver nitrate for 3 hours (silver-2 derivative); and 5 mM lead chloride for 4 hours (silver + lead derivative). Initial multiple isomorphous replacement (MIR) phases calculated with the PHASES program package (*33*) had a mean figure of merit of 0.48 to 2.0 Å, and they were improved by using Sayre's equation, density modification by histogram matching, and solvent flattening with the program SQUASH (*34*). The model was built into MIR electron density maps with the program CHAIN (*35*) and was refined with the program X-PLOR (*31*). An overall anisotropic temperature factor correction was applied to the native data set in the final stages of the refinement.

Item	Native	Silver-1	Silver-2	Silver + lead
Resolution (Å)	1.7	2.0	2.0	2.2
Observed reflections	20115	11320	11284	10201
Unique reflections	3950	2274	2547	1948
Data coverage (%)	98.9	87.4	98.3	99.1
R_{sym} (%)*	3.7	4.4	6.5	6.2
MIR analysis				
Resolution (Å)		2.0	2.0	2.2
Isomorphous difference†		0.069	0.102	0.128
Phasing power‡		1.73	1.64	0.73
Cullis *R* factor§		0.493	0.488	0.656
Refinement				
Resolution (Å)	6.0–1.7			
R factor‖	0.192			
Reflections with $\|F\| > 1\sigma$	3815			
Total number of atoms	306			
Water molecules	48			
rms on bond lengths (Å)¶	0.013			
rms on bond angles (°)¶	1.27			
rms on *B* values (Å^2)¶	5.4			

*$R_{sym} = \Sigma_h\Sigma_i|I_{h,i} - I_h|/\Sigma_h\Sigma_i I_{h,i}$, where I_h is the mean intensity of the i observations of the unique reflection h. †Isomorphous difference $= \Sigma|F_{PH} - F_P|/\Sigma F_{PH}$, where F_{PH} and F_P are the derivative and native structure factor amplitudes, respectively. ‡Phasing power $= \{\Sigma F_{H(calc)}^2/\Sigma|F_{PH(obs)} - F_{PH(calc)}|^2\}^{1/2}$. §Cullis *R* factor $= \Sigma|F_{PH} \pm F_P| - F_{H(calc)}|/\Sigma|F_{PH} - F_P|$ for centric reflections, where $F_{H(calc)}$ is the calculated heavy atom structure factor. ‖*R* factor $= \Sigma|F_{obs} - F_{calc}|/\Sigma F_{obs}$. ¶The rms deviation in *B* values is the rms deviation in the temperature factors between bonded atoms. The rms deviations for bond lengths and bond angles is the rms deviation from ideal stereochemical values.

Table 2. Summary of interactions between monomer A and monomers B, C, and D. Hydrogen bonds and salt links were assigned between polar or charged groups separated by less than 3.0 Å. Buried surface areas are those buried on monomer A by the other monomers, calculated with a spherical probe with a 1.7 Å radius (*36*). Interhelical angles were calculated from helix axes determined with the Cα atoms of residues 336 to 354. Interhelical distances represent the closest approach of the helical axes.

Item	Interactions with monomer		
	B	C	D
Van der Waals contacts	164	35	8
Hydrogen bonds	8	0	0
Salt links	2	2	0
Buried surface area (Å^2)	1138	360	108
Interhelical angles (°)	162	80	103
Interhelical distances (Å)	12.0	8.4	12.7

tetramer, each of the four monomers (A, B, C, and D) has three distinct interfaces with the other monomers. The A-B interface is more extensive than the A-C or A-D interfaces (Table 2), and the tetramer can therefore be regarded as a dimer formed through the association of the AB and CD dimers.

The monomers within the AB (or CD) dimer associate in a nearly antiparallel manner by means of their β strands and their α helices (Fig. 2). The strands form a highly twisted, two-stranded antiparallel β sheet, and the helices associate with a 161° angle, which is characteristic of other helix bundle proteins (*18*). In the dimer, the polypeptide chains are intertwined, with the β strand of A packing against the α helix of B. The association of the A and B monomers relies heavily on the eight backbone hydrogen bonds of the β sheet (Table 2). In addition, there is a small hydrophobic core consisting of the buried side chains of Ile^{332} and Phe^{341} and the partially buried side chains of Phe^{338} and Leu^{330} from each monomer (Fig. 3). We also observed an intermonomer salt link between Arg^{337} and Asp^{352} and an intermonomer hydrogen bond between Tyr^{327} and Arg^{333}.

The AB and CD dimers associate through their α helices to form the AB-CD tetramer (Fig. 2). The β strands are on the outside of the tetramer and are not involved in dimer-dimer interactions. The interactions between the two dimers are primarily hydrophobic in nature and involve the buried side chains of Ala^{347}, Phe^{341}, and Leu^{344} (Phe^{341} is also involved in the AB dimer hydrophobic core) and the partially buried side chains of Met^{340}, Leu^{348}, and Leu^{350} (Table 2 and Fig. 3). The helices from monomers A and C (or B and D) approach closely at Ala^{347} (Cα–Cα distance of 5.1 Å) across one of the symmetry axes. The short side chain of the alanine residue appears to be important for this interface because it allows for the close approach of the α helices. The A and C helices are "parallel" to each other but have a large interhelical angle of 81°. This arrangement of the helices is atypical of helix bundle or leucine zipper motifs where the helices have smaller interhelical angles.

The quaternary structure of the tetramer is very similar in all three crystal forms. The Cα atoms of the four helices in the tetragonal crystal form can be superimposed on those of the two hexagonal crystal forms with typical root-mean-square (rms) deviations of 0.9 Å for the helical regions (*19*). There is thus no indication that either crystallization conditions or crystal packing forces have perturbed the quaternary structure of the tetramer to any significant extent. However, we observed significant differences when we compared the crystal structure to a structure determined by nuclear magnetic resonance (NMR) spectroscopy (*20*) [see the technical comment in this issue for a discussion of the differences (*21*)]. A second NMR structure published recently (*22*) is more similar to our crystal structure (*23*).

The crystal structure presented in this report has implications for understanding why the oligomerization domain is rarely mutated in tumors, even though it appears to be necessary for p53's growth suppression activity. Less than 1% of the tumor-derived mutations are found in the tetramerization domain (*17*), and this has been interpreted to reflect selection for mutations which, while disrupting DNA binding, allow the mutant p53 to form inactive hetero-oligomers with the product of the remaining wild-type allele and to abrogate its function in a dominant negative fashion (*10, 24*). This gain of function has been demonstrated in cell culture by overexpressing the mutant proteins (*10, 25*), but it is not clear whether this effect contributes to neoplastic transformation and to the low frequency of tumor-derived mutations in this region.

An alternative hypothesis that is supported by the crystal structure is that few single amino acid mutations can adequately interfere with oligomerization to bring the DNA binding and transactivation activity of p53 below the threshold required for in vivo effects. Several observations support this hy-

pothesis. First, tetramerization of p53 may be redundant because dimerization appears to be sufficient for in vivo p53 activity. A dimeric p53 constructed by replacing the tetramerization domain with the coiled-coil dimerization domain of GCN4 has growth suppression activity like that of wild type (*12*). Second, the crystal structure of the tetramerization domain reveals that tetramerization involves two distinct dimerization interfaces, with one of the interfaces having extensive main chain hydrogen bonds (Fig. 3). It is conceivable, then, that most single amino acid changes cannot adequately destabilize both dimer interfaces to result in the complete dissociation to monomers. Third, whereas the majority of the mutations in the core DNA binding domain are missense mutations, those in the tetramerization domain are predominantly chain termination mutations [18 out of 22 mutations found in this region are either frameshift or chain termination mutations (*17*)]. Fourth, the NH_2-terminal transactivation domain of p53, which is essential for p53's growth suppression activity, is also rarely mutated in tumors. Systematic site-directed mutagenesis studies of this region have shown that two independent mutations are required to produce the same phenotype as a single tumor-derived mutation in the core DNA binding domain (*26*), making the inactivation of the transactivation domain a rare mutagenic event.

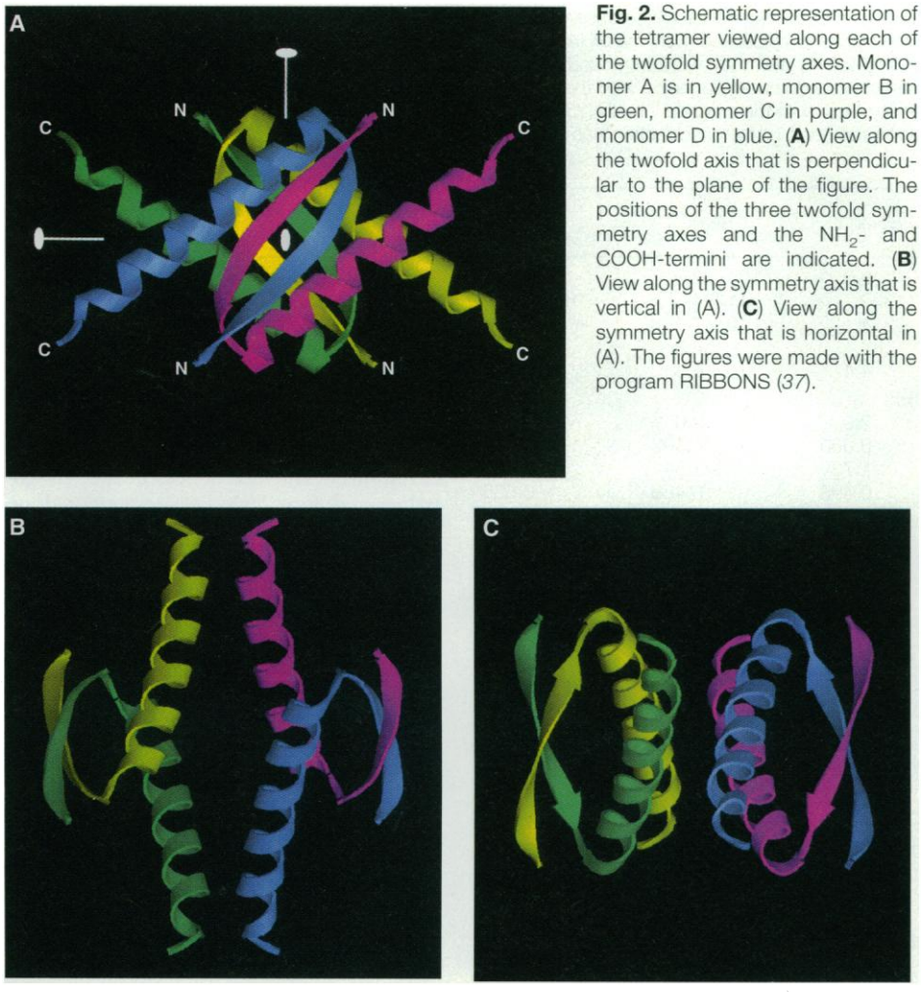

Fig. 2. Schematic representation of the tetramer viewed along each of the twofold symmetry axes. Monomer A is in yellow, monomer B in green, monomer C in purple, and monomer D in blue. (**A**) View along the twofold axis that is perpendicular to the plane of the figure. The positions of the three twofold symmetry axes and the NH_2- and COOH-termini are indicated. (**B**) View along the symmetry axis that is vertical in (A). (**C**) View along the symmetry axis that is horizontal in (A). The figures were made with the program RIBBONS (*37*).

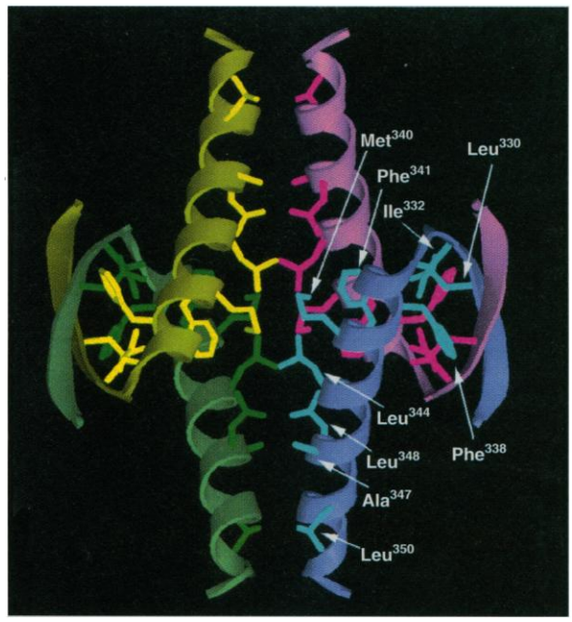

Fig. 3. Schematic representation of the tetramer showing the residues that make up the hydrophobic cores of the AB dimer and the AB-CD tetramer in the coloring scheme of Fig. 2. Eight side chains (four from each monomer) form the hydrophobic core at the AB dimer interface. Twenty side chains (five from each monomer) form the hydrophobic core at the AB-CD tetramer interface.

To obtain insights into the structure of the intact p53-DNA complex, we have constructed a model using the crystal structure of a dimeric p53 core domain–DNA complex published recently [residues 94 to 312 (*27*)], and the crystal structure of the tetramerization domain reported in this study (Fig. 4). In this model, four core domain molecules bind on the same face of the DNA, with their COOH-termini extending through the major groove and ending at the opposite face of the DNA. The tetramerization domains occur near the face of the DNA that is opposite to where the core domains bind. The arrangement of the four core domains is of lower symmetry than the arrangement of the four tetramerization domains, having only one twofold symmetry axis compared with the three mutually perpendicular twofold axes of the tetramerization domains. The core and oligomerization domains are connected through a 30-residue linker that is highly sensitive to proteolytic digestion and thus appears to be flexible or loosely folded (*7*). This linker can adequately span the distance between the core and oligomerization domains which, depending on the precise position and orientation of the oligomerization domain, could be 10 to 40 Å (a 30–amino acid peptide could be up to 100 Å long in a fully extended conformation). The length and apparent flexibility of the linker suggests that the oligomerization domains may not have a well-defined position and orientation with respect to the core domain–DNA complex.

The COOH-terminal portion of p53 has been shown to have an affinity for nucleic

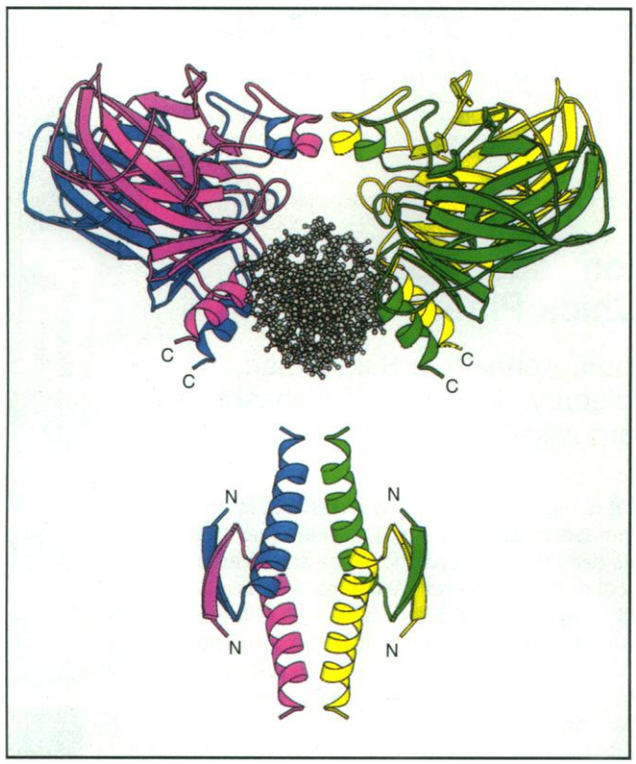

Fig. 4. Model of the core domain–DNA–tetramerization domain complex with the DNA axis perpendicular to the plane of the figure. The four core domains and the four tetramerization domains are colored separately and the DNA is colored gray. The model was constructed by using the crystal structure of the dimeric core domain–DNA complex (*27*), aligned on a B-form DNA model having a consensus tetrameric binding site (*2*), and the crystal structure of the oligomerization domain. The COOH-termini of the four core domains and the NH_2-termini of the tetramerization domains are indicated. The two domains are connected by means of a 30–amino acid long flexible linker, and it is likely that the oligomerization domain does not have a well-defined position with respect to the core domain–DNA complex.

acids. In particular, a 25–amino acid basic region immediately after the oligomerization domain has been proposed to interact nonspecifically with double- and single-stranded nucleic acids (*7*, *9*, *28*, *29*). In our model of the core domain–tetramerization domain–DNA complex (Fig. 4), the oligomerization domain is in close proximity to the DNA. This raises the possibility that the COOH-terminal portion of p53 may interact with DNA and may modulate the sequence-specific DNA binding activity. It has been proposed that the basic region may inhibit p53's sequence-specific DNA binding activity because deletion of the basic region or the binding of an antibody to this region appears to enhance DNA binding activity in vitro (*30*). Our model suggests that this inhibition may occur through the nonspecific interaction of the COOH-terminal region with the DNA. The basic regions could either mask the specific binding sites of the core domains, or they could interfere with the correct relative alignment of the two domains, for example, by intertwining the linker. In this respect, productive DNA binding by p53 may involve a competition between the sequence-specific DNA binding activity of the core domain and the nonspecific DNA binding activity of the COOH-terminal domain.

REFERENCES AND NOTES

1. A. J. Levine, J. Momand, C. A. Finlay, *Nature* **351**, 453 (1991); B. Vogelstein and K. W. Kinzer, *Cell* **70**, 523 (1992).
2. J. P. Bargonetti, N. Friedman, S. E. Kern, B. Vogelstein, C. Prives, *Cell* **65**, 1083 (1991); S. E. Kern *et al.*, *Science* **252**, 1708 (1991); W. D. Funk, D. T. Pak, R. H. Karas, W. E. Wright, J. W. Shay, *Mol. Cell. Biol.* **12**, 2866 (1992); W. S. El-Deiry, S. E. Kinzler, J. A. Pietenpol, K. W. Kinzler, B. Vogelstein, *Nature Genet.* **1**, 45 (1992).
3. S. Fields and S. K. Jang, *Science* **249**, 1046 (1990); L. Raycroft, H. Wu, G. Lozano, *ibid.*, p. 1049; G. Farmer *et al.*, *Nature* **358**, 83 (1992); T. Unger, M. M. Nau, S. Segal, J. D. Minna, *EMBO J.* **11**, 1383 (1992).
4. S. E. Kern *et al.*, *Science* **256**, 827 (1992).
5. M. B. Kastan *et al.*, *Cell* **71**, 587 (1992); Y. Yin, M. A. Tainsky, F. Z. Bischoff, L. C. Strong, G. M. Wahl, *ibid.* **70**, 937 (1992); L. R. Livingstone *et al.*, *ibid.*, p. 923; L. Hartwell, *ibid.* **71**, 543 (1992).
6. H. Hermeking and D. Eick, *Science* **265**, 2091 (1994); S. W. Lowe and H. E. Ruley, *Genes Dev.* **7**, 535 (1993); X. Wu and A. J. Levine, *Proc. Natl. Acad. Sci. U.S.A.* **91**, 3602 (1994); H. Symonds *et al.*, *Cell* **78**, 703 (1994).
7. N. P. Pavletich, K. A. Chambers, C. O. Pabo, *Genes Dev.* **7**, 2556 (1993).
8. J. Bargonetti, J. J. Manfredi, X. Chen, D. R. Marshak, C. Prives, *ibid.*, p. 2565.
9. Y. Wang *et al.*, *ibid.*, p. 2575.
10. E. Shaulian, A. Zauberman, D. Ginsberg, M. Oren, *Mol. Cell. Biol.* **12**, 5581 (1992).
11. H. W. Sturzbecher *et al.*, *Oncogene* **7**, 1513 (1992).
12. J. A. Pietenpol *et al.*, *Proc. Natl. Acad. Sci. U.S.A.* **91**, 1998 (1994).
13. When overexpressed, oligomerization-deficient p53 is capable of low levels of transactivation in transient transfection assays (*9*).
14. D. J. Park *et al.*, *Oncogene* **9**, 1899 (1994).
15. The initial identification of the tetramerization domain of p53 by proteolytic digestion has been described (*7*). A peptide corresponding to residues 311 to 367 of p53 was used in initial crystallization trials but failed to yield diffraction-quality crystals. Further digestion of the 311–367 peptide by subtilisin yielded a major fragment which was identified by NH_2-terminal sequencing and mass spectrometry to correspond to residues 320 to 356. This region of p53 is conserved across species (7 of the 32 residues are invariant, and many of the remaining ones involve conservative substitutions) and is delimited by sequences that are variable and contain deletions and insertions in other species (*16*). The proteolytic fragment was purified to near homogeneity according to procedures reported for the 311–367 peptide (*7*), and it yielded three crystal forms in hanging drop vapor diffusion crystallization experiments. A tetragonal form in space group *P*422 ($a = b = 45.45$ Å, and $c = 33.03$ Å) was grown from 3 M sodium formate, 0.5 M ammonium sulfate, and 50 mM tris-HCl (pH 8.8); a hexagonal form (form I) in space group $P6_122$ ($a = b = 79.8$ Å, and $c = 49.9$ Å) was grown from 6 M sodium formate, and 100 mM Hepes-Na^+ (pH 7.5); and a second hexagonal form (form II) in space group $P6_122$ ($a = b = 138.6$ Å, and $c = 49.9$ Å) was grown from 28% polyethylene glycol (PEG) 400 and 100 mM Hepes-Na^+ (pH 7.5). The tetragonal crystal form contained one monomer per asymmetric unit and diffracted to beyond 1.7 Å resolution. Hexagonal form I contained one dimer (AB dimer) per asymmetric unit and diffracted to 2.8 Å. Hexagonal form II contained three dimers (AB dimers) per asymmetric unit and diffracted to 3.0 Å. The structure of the tetragonal form was determined by the MIR method, and the statistics from the crystallographic analysis are presented in the text. The structure of the hexagonal form I was also determined by the MIR method. Briefly, we calculated MIR phases for the hexagonal form I by using four heavy atom derivatives (lead chloride, samarium acetate, silver nitrate, and dipotassiumhexabromoplatinate), and the phases had a mean figure of merit of 0.49 at 3.0 Å resolution. Solvent-flattened MIR maps had clear electron density for the helical residues 336 to 352 but had poor electron density for the β sheet region. The structure has been partially refined with X-PLOR (*31*) and has a crystallographic *R* factor of 29.9% for 6.0 to 2.9 Å data (1845 reflections with $|F| > 2\sigma$; rms deviation in bond lengths = 0.020 Å, and in bond angles = 2.2°). The β sheet region, which had poor electron density in the MIR map, has high temperature factors in the partially refined model, and it appears to be disordered in the hexagonal crystal form I (we presume that this is due to the lack of crystal-packing contacts in this region). The structure of the hexagonal form II was determined by molecular replacement with the programs MERLOT and BRUTE (*32*), with the dimer model from the hexagonal form I crystal structure. In the hexagonal form II structure the α helices are well defined, but the β sheet regions exhibit the same disorder apparent in the hexagonal form I structure.
16. T. Soussi, C. C. Fromentel, P. May, *Oncogene* **5**, 945 (1990).
17. M. S. Greenblatt, W. P. Bennett, M. Hollstein, C. C. Harris, *Cancer Res.* **54**, 4855 (1994); Database of p53 mutations, European Molecular Biology Laboratory Data Library (1994).
18. D. W. Banner, M. Kokkinidis, D. Tsernoglou, *J. Mol. Biol.* **196**, 657 (1987).
19. Only the Cα atoms of the helices (residues 338 to 350) were used in the superposition because the β sheet regions appear to be partially disordered in the hexagonal crystal forms.
20. G. M. Clore *et al.*, *Science* **265**, 386 (1994).
21. G. M. Clore *et al.*, *ibid.* **267**, 1515 (1995).
22. W. Lee *et al.*, *Nature Struct. Biol.* **1**, 877 (1994).
23. The initial NMR structure (*20*) has a rms deviation of Cα atoms of 3.1 Å when superimposed on the crystal structure (residues 325 to 350). This deviation is primarily due to a 36° difference in the orientation of the AB dimer relative to the CD dimer. A revision of that structure (*21*) has a rms deviation of only 1.2 Å. The second NMR structure published recently (*22*) has a rms deviation of 1.5 Å.
24. J. Milner and E. A. Medcalf, *Cell* **65**, 765 (1991).
25. P. Hinds, C. Finlay, A. J. Levine, *J. Virol.* **63**, 739 (1989); P. W. Hinds *et al.*, *Cell Growth Differ.* **1**, 571 (1990); O. Halvey, D. Michalovitz, M. Oren, *Science* **250**, 113 (1990); D. Dittmer *et al.*, *Nature Genet.* **4**, 42 (1993).
26. J. Lin, J. Chen, B. Elenbaas, A. J. Levine, *Genes Dev.* **8**, 1235 (1994).
27. Y. Cho, S. Gorina, P. D. Jeffrey, N. P. Pavletich, *Science* **265**, 346 (1994).
28. P. Oberosler, P. Hloch, U. Ramsperger, H. Stahl, *EMBO J.* **12**, 2389 (1993).
29. L. Wu, H. J. Bayle, B. Elenbaas, N. P. Pavletich, A. J. Levine, *Mol. Cell. Biol.*, **15**, 497 (1995).
30. T. R. Hupp, D. W. Meek, C. A. Midgley, D. P. Lane,

Cell **71**, 875 (1992).
31. A. T. Brünger, J. Kuriyan, M. Karplus, *Science* **235**, 458 (1987); A. T. Brünger, *X-PLOR v3.1 Manual* (Yale Univ. Press, New Haven, CT, 1990).
32. P. M. D. Fitzgerald, *J. Appl. Crystallogr.* **21**, 273 (1988); M. Fujinaga and R. J. Read, *ibid.* **20**, 273 (1987).
33. W. Furey and S. Swaminathan, *Am. Crystallogr. Assoc. Meet. Abstr. Ser. 2* **18**, 73 (1990).
34. K. Y. J. Zhang, *Acta Crystallogr.* **D49**, 213 (1993).
35. J. S. Sack, *J. Mol. Graph.* **6**, 224 (1988).
36. M. L. Connolly, *J. Appl. Crystallogr.* **16**, 548 (1983).
37. M. Carson, *ibid.* **24**, 958 (1991).
38. Supported by National Cancer Institute grant CA08748-29, the Dewitt Wallace Foundation, and the Pew Charitable Trusts (N.P.P.). Coordinates have been deposited with the Brookhaven Protein Data Bank.

4 November 1994; accepted 12 January 1995

Pineal Opsin: A Nonvisual Opsin Expressed in Chick Pineal

Marianna Max,* Peter J. McKinnon, Kenneth J. Seidenman, R. Keith Barrett, Meredithe L. Applebury, Joseph S. Takahashi, Robert F. Margolskee

Pineal opsin (P-opsin), an opsin from chick that is highly expressed in pineal but is not detectable in retina, was cloned by the polymerase chain reaction. It is likely that the P-opsin lineage diverged from the retinal opsins early in opsin evolution. The amino acid sequence of P-opsin is 42 to 46 percent identical to that of the retinal opsins. P-opsin is a seven-membrane spanning, G protein–linked receptor with a Schiff-base lysine in the seventh membrane span and a Schiff-base counterion in the third membrane span. The primary sequence of P-opsin suggests that it will be maximally sensitive to ~500-nanometer light and produce a slow and prolonged phototransduction response consistent with the nonvisual function of pineal photoreception.

All identified vertebrate opsins fit into four major groups based on conservation at the protein level, epitomized by chick green, blue, violet, and red opsins (*1*, *2*). The order of divergence of these groups is not well resolved. The green opsin cluster contains as a subgroup the rod opsins (rhodopsin) used for scotopic vision (*2*). Within the red cluster multiple duplication events gave rise to closely related "green" opsins in Old World primates and some fish (*3*). Opsins within a given class share ~65 to 95% amino acid identity, whereas identity among classes is only ~40 to 50%.

The chick pineal is thought to contain a rhodopsin-like photoreceptor with a maximal sensitivity at 500 nm (*4*), based on the action spectrum for light-induced suppression of *N*-acetyltransferase activity, which reduces melatonin synthesis. Two other pieces of evidence also suggest that the pineal gland contains an opsin-like protein: (i) Vitamin A depletion from cultured pineal cells reduces light-mediated suppression of melatonin synthesis, suggesting the action of a vitamin A–based pigment (*5*) (presumably an opsin-bound chromophore) and (ii) immunocytochemistry indicates the presence of one or more opsin-like proteins in avian pinealocytes (*6*).

To identify the opsin or opsins expressed in pineal, we used degenerate oligonucleotide primers and reverse transcriptase–polymerase chain reaction (RT-PCR) (*7*) to amplify and clone opsin-like complementary DNAs (cDNAs) from chick pineal. Using primers to conserved regions flanking the Schiff-base lysine in the seventh transmembrane domain, we recovered three distinct opsin-like cDNAs: chick red opsin, chick green opsin, and a previously unidentified opsin [pineal opsin (P-opsin)]. Ribonuclease (RNase) protection (*8*) detected abundant P-opsin RNA but no retinal opsin RNAs in pineal (Fig. 1A) (*9*). RNase protection detected no expression of P-opsin transcript in chick retinal RNA although, as expected, red, green, blue, violet, and rhodopsin transcripts were detected. Neither P-opsin nor retinal opsin RNAs were detected in chick brain by RNase protection. In situ hybridization (*10*) demonstrated expression of P-opsin in most pinealocytes (Fig. 1, B and C), but not in chick retina. Thus, P-opsin is an abundant pineal transcript absent from retina.

A pineal-specific cDNA library was

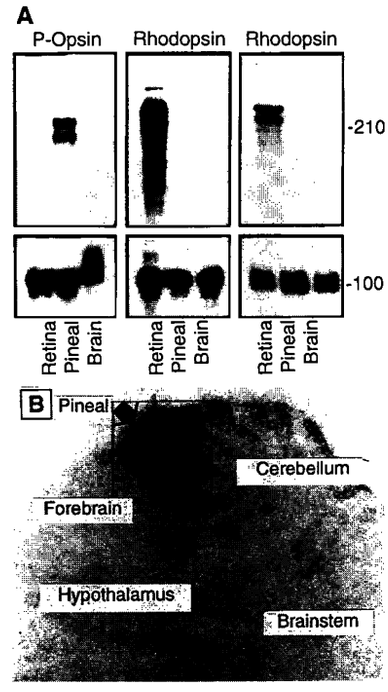

Fig. 1. Expression of P-opsin mRNA. (**A**) RNase protection assay (*8*) with RNA (~30 μg) from chick pineal, retina, or brain. (Left) Exposure for 8 hours shows abundant P-opsin expression in pineal but no expression elsewhere. (Middle) Eight-hour exposure shows that rhodopsin is not expressed in pineal; however, its protected product in retina appears to smear due to overexposure. (Right) Four-hour exposure of the rhodopsin protection shows the appropriate P-opsin bands in retina at ~210 bp. In other RNase protection assays, protected products were detected with probes made from chick green, red, blue, and violet opsins in retinal RNA but not in pineal RNA. All probes include 70 bp of vector sequence: No full-length probe could be detected after RNase digestion, indicating that only sequence-specific probe fragments of the correct size were protected. All protections included an actin standard (100-bp product) to control the amount of target RNA in each assay. (**B**) Autoradiograph of in situ hybridization (*10*) of ^{33}P-labeled P-opsin probe to a sagittal section of chick brain including attached pineal. The dotted square around the pineal gland corresponds to the view in (C). (**C**) Dark field view (40× magnification) of the boxed area of the section in (B) after the slide was dipped in emulsion (NTB 2 from Kodak), exposed for 2 weeks, and developed. The label is restricted to the pineal. Retina is not labeled by this probe and the sense probe control does not label the brain, pineal, or retina.

M. Max, Roche Institute of Molecular Biology, Roche Research Center, Hoffmann-LaRoche, Nutley, NJ 07110, USA, and National Science Foundation Center for Biological Timing, Department of Neurobiology and Physiology, Northwestern University, 2153 North Campus Drive, Evanston, IL 60208, USA.
P. J. McKinnon and R. F. Margolskee, Roche Institute of Molecular Biology, Roche Research Center, Hoffmann-LaRoche, Nutley, NJ 07110, USA.
K. J. Seidenman, R. K. Barrett, J. S. Takahashi, National Science Foundation Center for Biological Timing, Department of Neurobiology and Physiology, Northwestern University, 2153 North Campus Drive, Evanston, IL 60208, USA.
M. L. Applebury, Harvard Medical School, Howe Laboratories, 243 Charles Street, Boston, MA 02114, USA.
*To whom correspondence should be addressed.